Supplementary Information (SI) for Journal of Materials Chemistry A.

Single-Ion Conductor Gel Polymer Electrolytes Enabling Anionic-Polymer-Induced Solid Electrolyte Interphase for Dendrite-Free Lithium-Metal Batteries

Ping-Hui Duan, Guo-Rui Zhu, Jia-Ling Yu, Zhe Guan, Gang Wu, Xiu-Li Wang*, Yu-Zhong Wang*

The Collaborative Innovation Center for Eco-Friendly and Fire-Safety Polymeric Materials (MoE), National Engineering Laboratory of Eco-Friendly Polymeric Materials (Sichuan), State Key Laboratory of Polymer Materials Engineering, College of Chemistry, Sichuan University, Chengdu 610064, China

E-mail: gangwu@scu.edu.cn, wangxiuli@scu.edu.cn.

1. Experimental

1.1 Materials

Lithium hydroxide, 5-aminosalicylic acid, boric acid, and poly(ethylene glycol) diglycidyl ether (PEGDE) were purchased from Aladdin Industrial Co., Ltd. (Shanghai, China). Gamma-butyrolactone (GBL) was purchased from Macklin Reagent (Shanghai, China). Cellulose membrane (NKK TF4030) was purchased from Canrd New Energy Technology Co., Ltd. (Dongguan, China). $LiFePO_4$, acetylene black, and Poly (vinylidene fluoride) (PVDF) were obtained from Shenzhen Kejing Star Technology Co., Ltd. (Shenzhen, China). All the materials were used directly without further purification.

1.2 Preparation of LiB5AB and SIGPEs@NKK

lithium bis (5-Aminosalicylic acid) borate (LiB5AB) was synthesized according to the procedure described in Figure S1. 0.39 g of Lithium hydroxide (16.5 mmol), 5.00 g of 5-aminosalicylic acid (33 mmol), and 1.01 g of boric acid (16.5 mmol) were added to acetonitrile and heated at 80 °C. A light brown solid powder was collected by filtration. The ^{1}H, ^{11}B NMR, and mass spectra of LiB5AB are shown in Figure S2.

The $SIGPE_{0.3}$@NKK was prepared by in-situ polymerization of precursor solution composed of crosslink node LiB5AB (0.64 g, 2 mmol), linker PEGDE (1.424 g, 0.712 mmol), and solvent GBL. LiB5AB and PEGDE were dissolved in GBL with constant stirring until completely dissolved. To investigate the effect of different epoxy: amine molar ratios on the polymer structure, the proportions of LiB5AB, PEGDE, and GBL were systematically varied. All processes of electrolyte preparation were conducted in an Ar-filled glove box (LS-750s, Chengdu Dellix Industry Co. Ltd., $[O_2] < 0.1$ ppm, $[H_2O] < 0.1$ ppm). After the injection of the precursor solution, the battery was heated at 80 ℃ for 2 h.

1.3 Characterization

The polymerization process of epoxy groups and amino groups was carried out using TA Q200 DSC at a heating rate of 3 °C min^{-1} under nitrogen. Fourier transform infrared spectroscopy (FT-IR) was recorded with Nicolet 6700 spectrometer. The surface morphology of NKK, $SIGPE_{0.3}$@NKK, and Li anode was characterized by scanning electron microscopy (SEM) and energy dispersive X-ray spectroscopy (EDX) (Phenom proX). The composition of the cycled lithium surface was conducted by X-ray photoelectron spectra (XPS, Kratos Axis Ultra) with a standard Al Kα X-ray source. Mechanical properties were carried out from stress-strain tests by INSTRON F563-44 using a dumbbell shape of 20 mm (long) × 4 mm (width) × 120 μm (thickness) at a speed of 5mm min^{-1}. A NETZSCH 209 F1 instrument was used to investigate the thermogravimetric analysis (TGA) of polymer electrolytes at a heating rate of 10 °C min^{-1} under nitrogen.

1.4 Electrochemical characterizations

The electrochemical impedance spectrum of batteries with SIGPEs@NKK was measured by an electrochemical workstation (CHI600E) in the frequency range of 1 Hz to 10^5 Hz, and the ionic conductivity was calculated by the following equation:

$$\sigma = \frac{l}{SR} \tag{3}$$

l is the thickness of the polymer electrolyte, R is the bulk resistance recorded by electrochemical impedance spectroscopy (EIS), and S is the area of the stainless steel sheets.

The activation energy (Ea) for Li^+ transport was obtained from the Arrhenius equation:

$$\mathrm{Ea} = \mathrm{RT} \ln \frac{\mathrm{A}}{\sigma} \tag{4}$$

Where R is the molar gas constant (8.314 J mol^{-1} K^{-1}), T is the temperature of operation, A is the pre-exponential factor, and σ is the ionic conductivity.

The electrochemical stability window was examined by linear sweep voltammetry (LSV) using Li||SS cells at a scan rate of 1 mV s^{-1} between 0-6 V. The reversibility of Li stripping/plating was carried out by cyclic voltammetry (CV) using a Li| SIGPE0.3@NKK |$LiFePO_4$ cell in the voltage range of 2.5-4.2 V at a scanning rate of 1 mV s^{-1}. The compatibility of $SIGPE_{0.3}$@NKK with a Li anode was using a galvanostatic cycling measurement with a Li|$SIGPE_{0.3}$@NKK|Li symmetric cell under different current densities, and each charge/discharge cycle lasts for 1 h.

The lithium-ion transference number (t_{Li+}) was measured by the combination of electrochemical impedance spectroscopy and chronoamperometry method on Li|SIGPE0.3@NKK|Li symmetric cell, and the t_{Li+} can be obtained from the following equation :

$$\mathrm{t_{Li+}} = \frac{I_{SS}(\Delta V - I_0 R_0)}{I_0(\Delta V - I_{SS} R_{SS})} \tag{5}$$

Where the I_0 and I_{SS} represent the current of Li|SIGPE0.3@NKK|Li cell at initial state and steady-state, respectively. R_0 and R_{SS} are the resistance of

Li|SIGPE0.3@NKK|Li cell before and after the polarization process, respectively, and the applied polarization (ΔV) was 10 mV.

The molecular dynamics were performed using the software package GROMACS (version 2021.3) [1-4]. The molecules were optimized in ORCA in B97-3C level first. The system was constructed by packmol [5], and concomprised specific molecules in a cubic box with the edge size of 5 nm. The atomic interactions were parameterized by the optimized potentials for liquid simulations all-atom (OPLS-AA) force field [6][6], and RESP2 charge obtained from Multiwfn [7] was applied in the calculations. After the energy minimization, the systems were pre-balanced in NPT ensemble with Berendsen method for 1 ns. Then, the production run was carried out in the NPT ensemble at 300 K with the time step of 1 fs. The temperature of the system was controlled by a V-rescale thermostat (τ_T=1 ps), and the Parrinello-Rahman . pressure coupling (τ_p=2 ps) was used to control the pressure. After 20 ns of simulation, the RDF of the particles were analyzed by the toolkits of GROMACS.

Density functional theory (DFT) calculations for Li^+-$O_{polymer}$ and Li^+-O_{GBL} were obtained from the the ORCA (version 5.0.4) software package [8, 9]. Geometry optimizations and single-point energy calculations were performed using RI-B3LYP-D3(BJ) function with def2-TZVP basis set. To account for dispersion interactions, the DFT-D3 correlation correction was included in the calculations. This correction accounts for the long-range dispersion forces that are not adequately captured by standard DFT functionals. The D3 correction was applied with the Becke-Johnson damping scheme. The counterpoise method is used to correct the basis set superposition error (BSSE) in quantum chemistry calculations. BSSE arises when the basis set of one molecule overlaps with the basis set of another, leading to an overestimation of the interaction energy between them. The binding energy ΔE_{bind} is defined as the following equation:

$$\Delta E_{bind} = E(AB) - E(A) - E(B) + E_{BSSE} \qquad (6)$$

Where the ΔE_{bind} was the binding energy of A and B. E_{A+B} was the total energy of A combined with B. E_A and E_B were independent energies of A and B, E_{BSSE} was the energy of basis set superposition error, respectively.

The $LiFePO_4$ cathode was made up of $LiFePO_4$ (80 wt%), Super P (10 wt%), and PVDF (10 wt%) on an aluminum collector, and the active material weight of this cathode is 1.6 mg cm^{-2}. The rate capability and cycle life of Li| $SIGPE_{0.3}$@NKK |$LiFePO_4$ cell were performed on the battery testing system (Shenzhen Neware Electronics Co., Ltd), and the voltage ranges of 2.5~4.2 V. A $LiFePO_4$| $SIGPE_{0.3}$@NKK |Li pouch cell was assembled by a commercial $LiFePO_4$ cathode (3.5×4.5 cm^2), $SIGPE_{0.3}$@NKK (4.0×5.0 cm^2) and Li foil (3.5×4.5 cm^2).

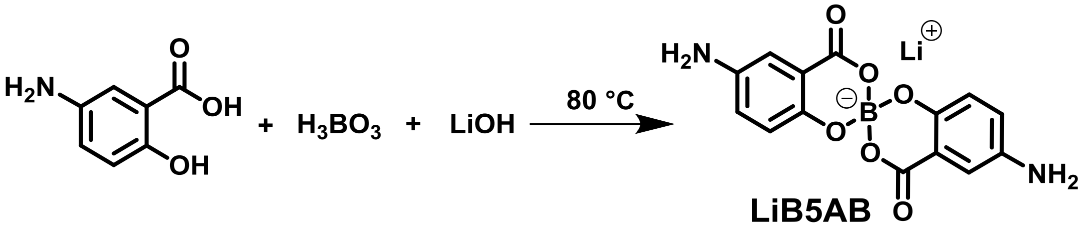

Figure S1. Synthesis routes of lithium bis (5-Aminosalicylic acid) borate (LiB5AB)

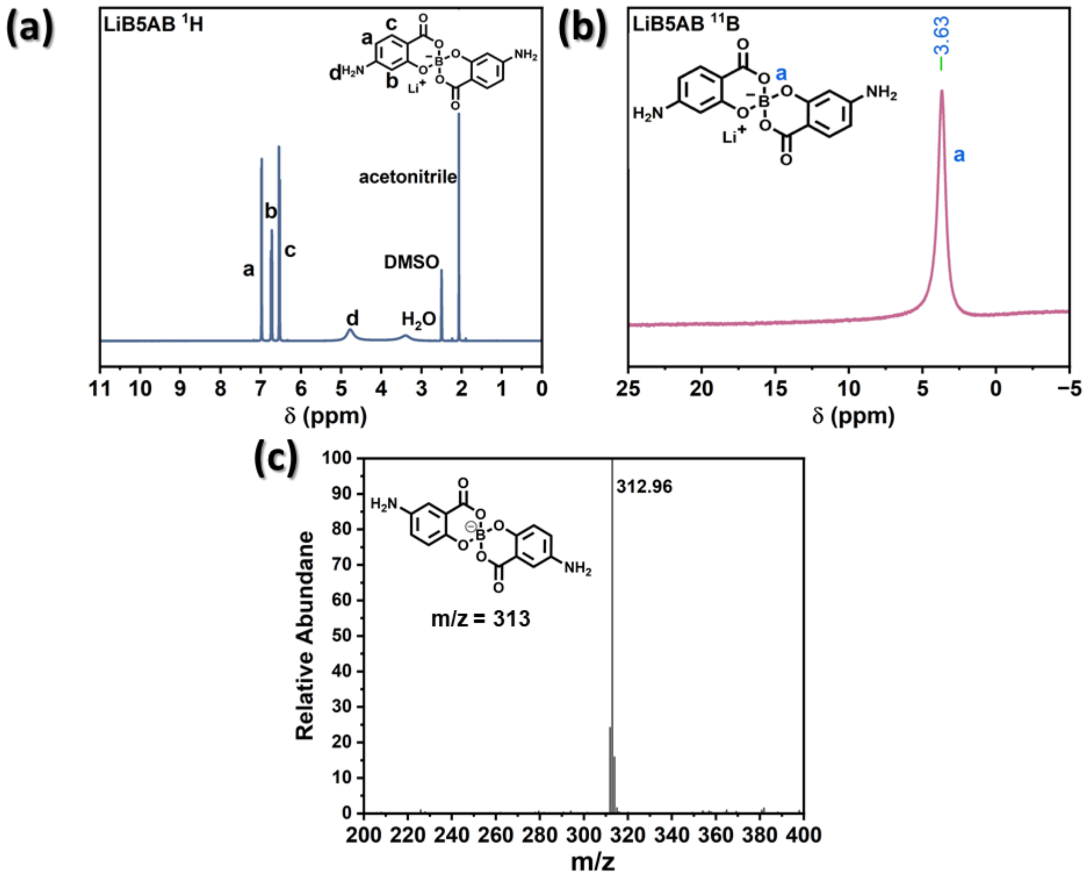

Figure S2. (a) ^{1}H NMR and (b) ^{11}B NMR spectra of LiB5AB. (c) Mass spectrum of LiB5AB.

Table S1. Physical properties of some organic solvents commonly used in rechargeable lithium-ion batteries.

	Melting point (°C)	**Boiling point (°C)**	**Dielectric permittivity**	**Viscosity at 25 °C (mPa S)**
DMC	**2.4**	**90**	**3.1**	**0.58**
DEC	**-43**	**125**	**2.9**	**0.75**
EMC	**-55**	**108**	**2.8**	**2.4**
EC	**36.4**	**248**	**89.6**	**1.9（40 °C）**
PC	**-48.8**	**242**	**66**	**2.5**
GBL	**-43.5**	**205**	**39**	**1.73**

We selected GBL as the solvent for several reasons: Firstly, the solvents help solvate Li^+ ions and facilitate their transportation. Therefore, it is required that the solvents have a high dielectric permittivity but a low viscosity. The lithium salt (LiB5AB) exhibits strong polarity, which results in low solubility in typical linear carbonate solvents like dimethyl carbonate (DMC), diethyl carbonate (DEC), and ethyl methyl carbonate (EMC) due to their low dielectric permittivity (**Table S1**). Among cyclic carbonate solvents, ethylene carbonate (EC) is solid at room temperature and propylene carbonate (PC) has high viscosity, both of which hinder efficient ion conduction at room temperature.In contrast, GBL offers a wide liquid range, lower viscosity, and excellent solubility for LiB5AB, which are beneficial for facilitating ion mobility. Based on these considerations, we chose GBL as a solvent for our study.

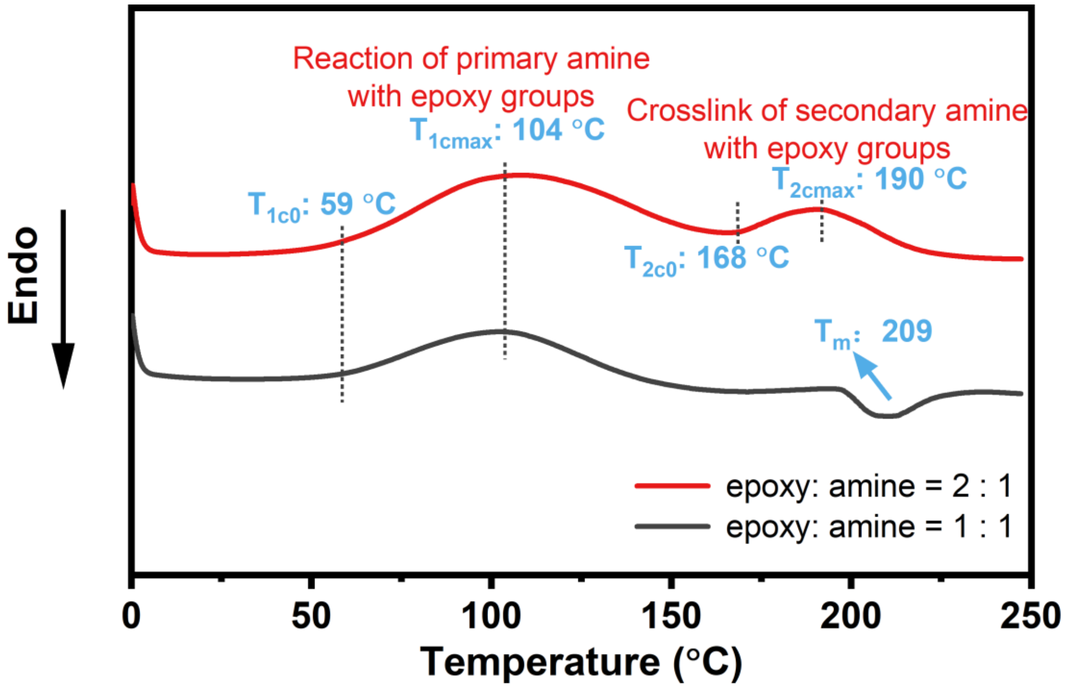

Figure S3. DSC curves of the precursor with different epoxy: amine ratios. T_{1c0} and T_{1cmax} represent the onset temperature and the temperature of the peak maximum of crosslinking of primary amines and epoxy groups, respectively. T_{2c0} and T_{2cmax} represent the onset temperature and the temperature of the peak maximum of crosslinking of secondary amines and epoxy groups. T_m represents the melting temperature of the linear polymer.

During the heating process, it can be observed that the precursor with an epoxy: amine ratio of 2:1 exhibits two exothermic peaks, corresponding to the reactions of primary amine with epoxy groups, and the subsequent reaction of secondary amine with epoxy groups to form crosslinked polymers. On the other hand, the precursor with an epoxy: amine ratio of 1:1 only shows one exothermic peak during the heating process, corresponding to the crosslinking of primary amine and epoxy groups. At higher temperatures, an endothermic peak appears, corresponding to the melting of the previously formed polymer. These results indicate that the precursor with an epoxy:

amine ratio of 1:1 generates linear polymers, while the precursor with an epoxy: amine ratio of 2:1 generates crosslinked polymers.

Table S2. DSC data of the precursor with different epoxy: amine ratios.

epoxy:amine	**primary amine**		**secondary amine**	
	T_{1c0} (°C)	T_{1cmax} (°C)	T_{2c0} (°C)	T_{2cmax} (°C)
1 : 1	59	104	168	190
2 : 1	59	104	-	-

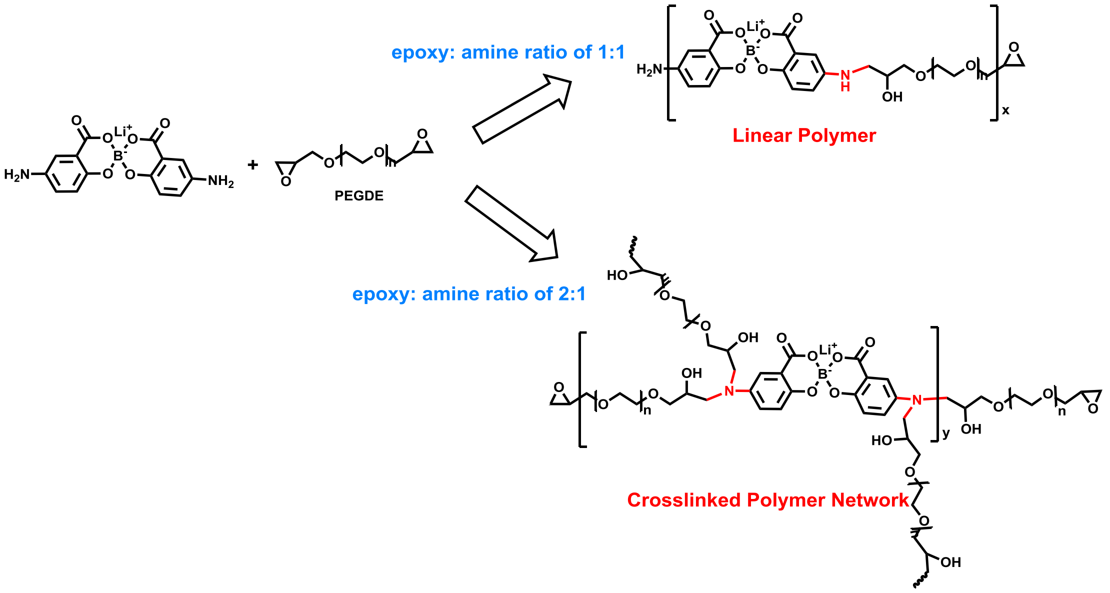

Figure S4. According to the DSC results, it is inferred that different products are obtained from the preparation of precursors with different epoxy: amine ratios.

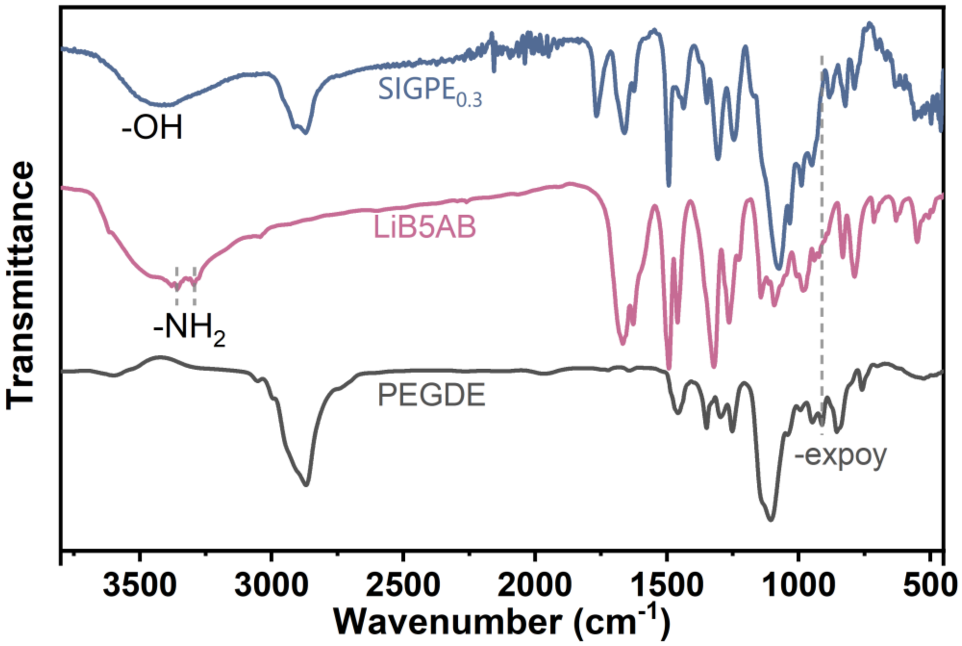

Figure S5. FT-IR spectra of LiB5AB, PEGDE, and SIGPE.

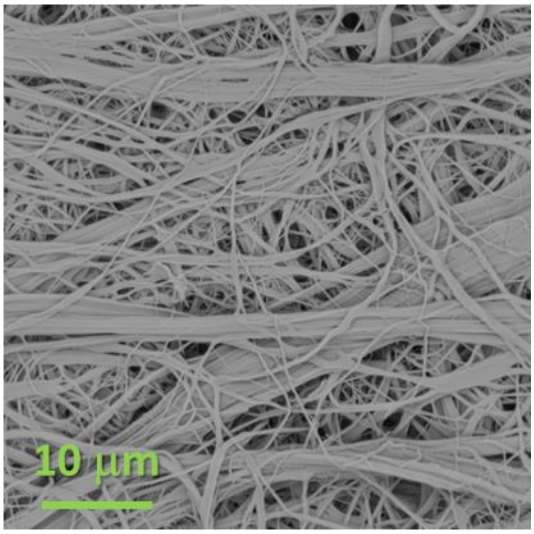

Figure S6. SEM image of the NKK membrane.

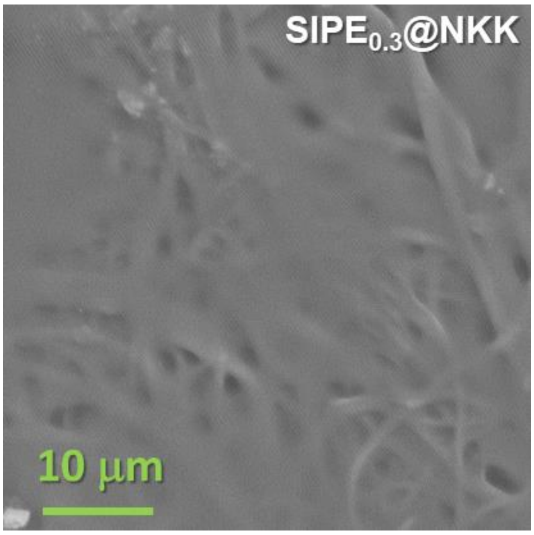

Figure S7. SEM image of the SIGPE@NKK membrane.

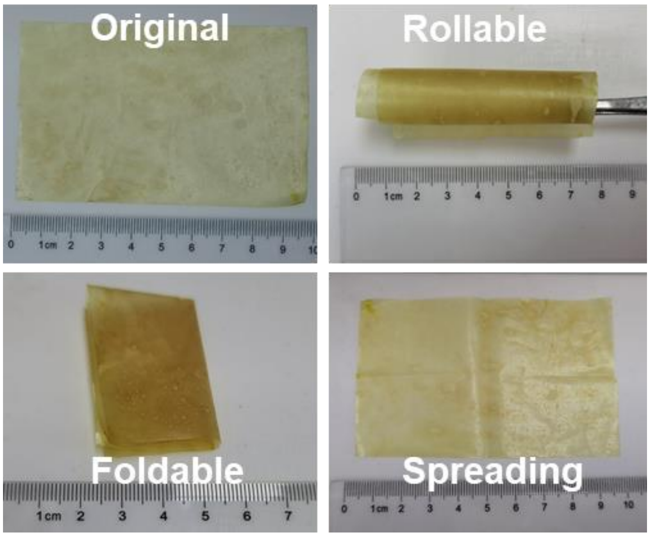

Figure S8. Photographs of the SIGPE@NKK in fold, scrunch, and spread states.

Table S3. Polymerization conditions of SIGPEs prepared with different concentrations of precursors, and the state of precursors before and after polymerization. (According to the concentration of precursor solution, those SIGPEs were denoted as SIGPE$_{1.5}$, SIGPE$_{1.0}$, SIGPE$_{0.75}$, SIGPE$_{0.5}$, and SIGPE$_{0.3}$, respectively)

	SIGPE$_{1.5}$	**SIGPE$_{1.0}$**	**SIGPE$_{0.75}$**	**SIGPE$_{0.5}$**	**SIGPE$_{0.3}$**
C$_{(LiB5AB)}$ / mol·L^{-1}	1.5	1.0	0.75	0.5	0.3
n$_{(5\text{-}ALB)}$ / mmol	1.5				
V$_{(GBL)}$ / mL	1.0	1.5	2.0	3.0	5.0
polymerization condition	60°C、2h	60°C、2h	80°C、2h	80°C、2h	80°C、2h
Before polymerization	LiB5AB does not dissolve completely		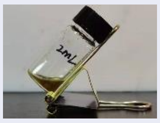		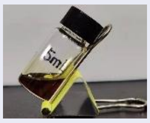
After polymerization	-	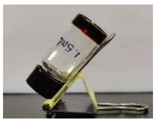	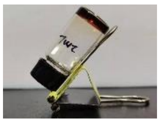		

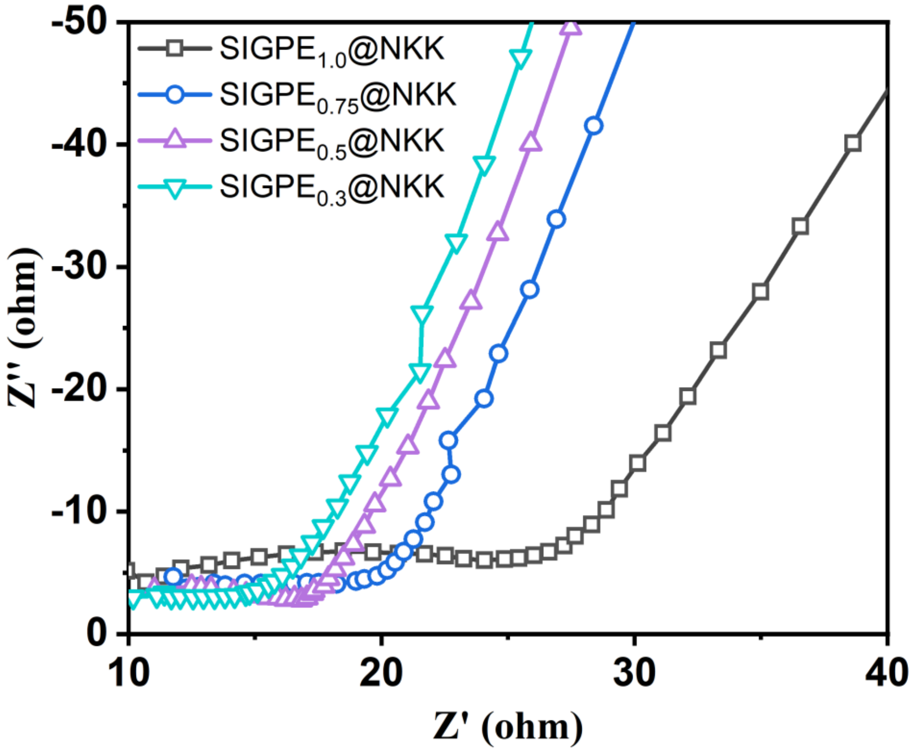

Figure S9. Nyquist plots of the symmetric cells with SIGPE$_{1.0}$@NKK, SIGPE$_{0.75}$@NKK, SIGPE$_{0.5}$@NKK, and SIGPE$_{0.3}$@NKK.

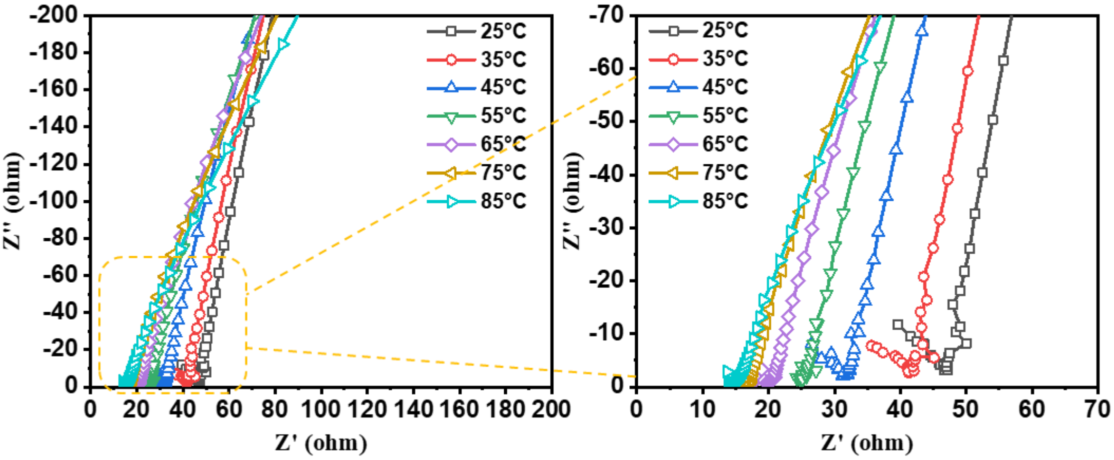

Figure S10. The EIS spectra of SIGPE$_{0.3}$@NKK at different temperatures.

Table S4. The ionic conductivity and respective parameters of SIGPE$_{0.3}$@NKK at various temperatures.

	Temperature (T)						
	25 °C	35 °C	45 °C	55 °C	65 °C	75 °C	85 °C
1000/T	3.35	3.24	3.14	3.04	2.95	2.87	2.79
Log(σ)	-4.44	-4.38	-4.26	-4.16	-4.07	-3.99	-3.93

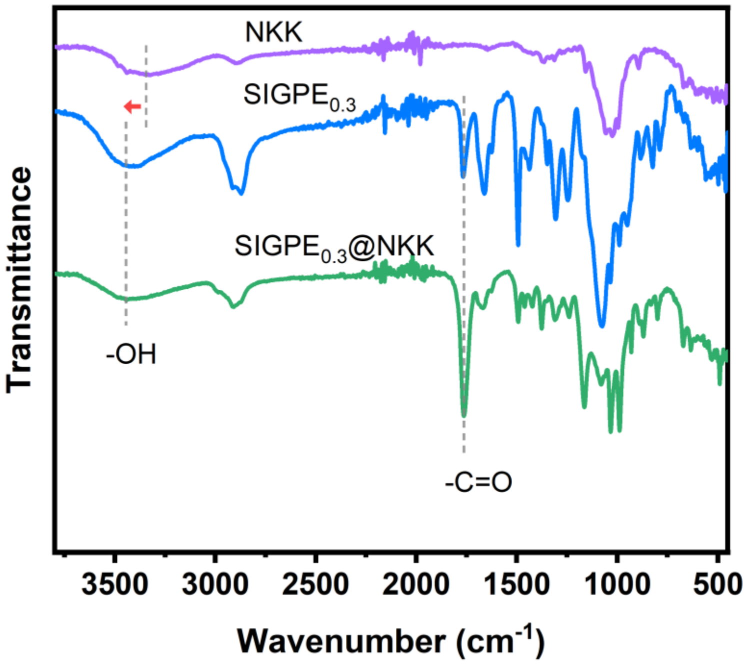

Figure S11. FT-IR spectra of SIGPE$_{0.3}$@NKK, SIGPE$_{0.3}$, and NKK cellulose membrane.

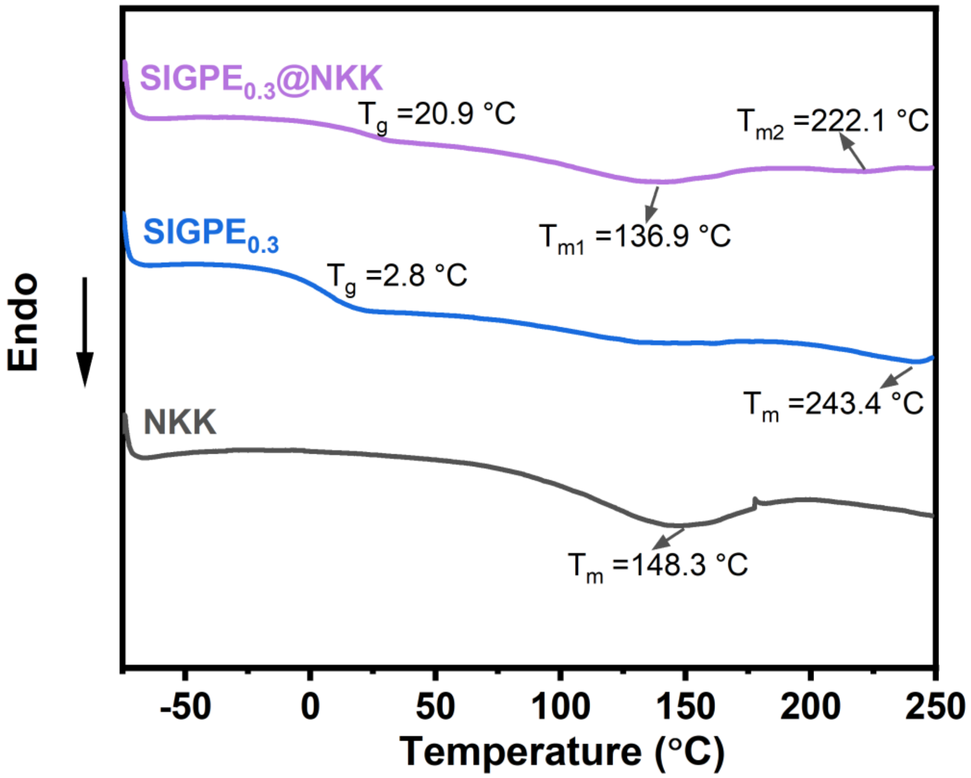

Figure S12. DSC cruves of SIGPE$_{0.3}$@NKK, SIGPE$_{0.3}$, and NKK cellulose membrane.

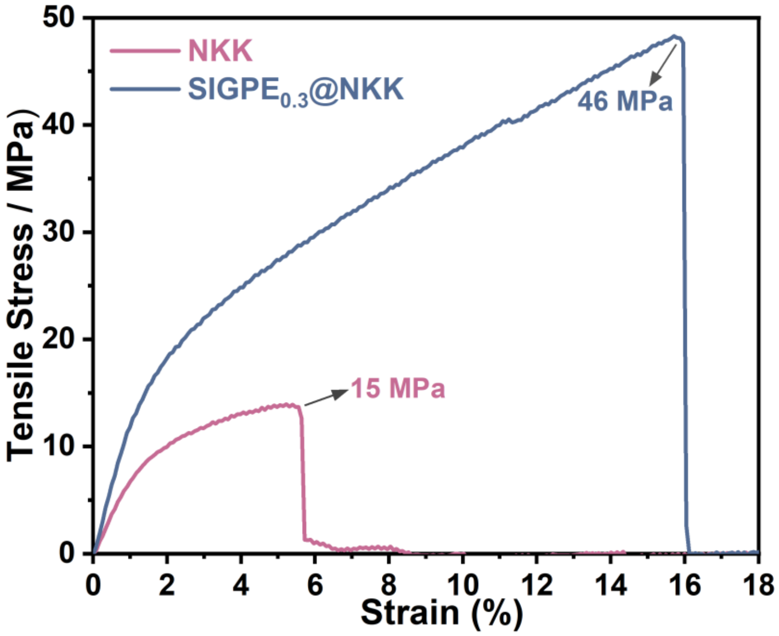

Figure S13. Strain and stress curves of NKK and SIGPE$_{0.3}$@NKK.

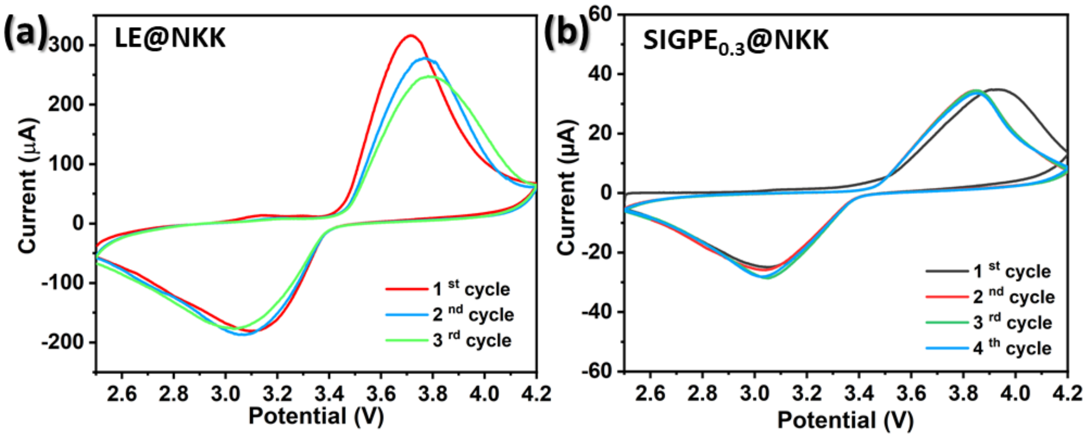

Figure S14. CV cruves of LE@NKK and SIGPE$_{0.3}$@NKK.

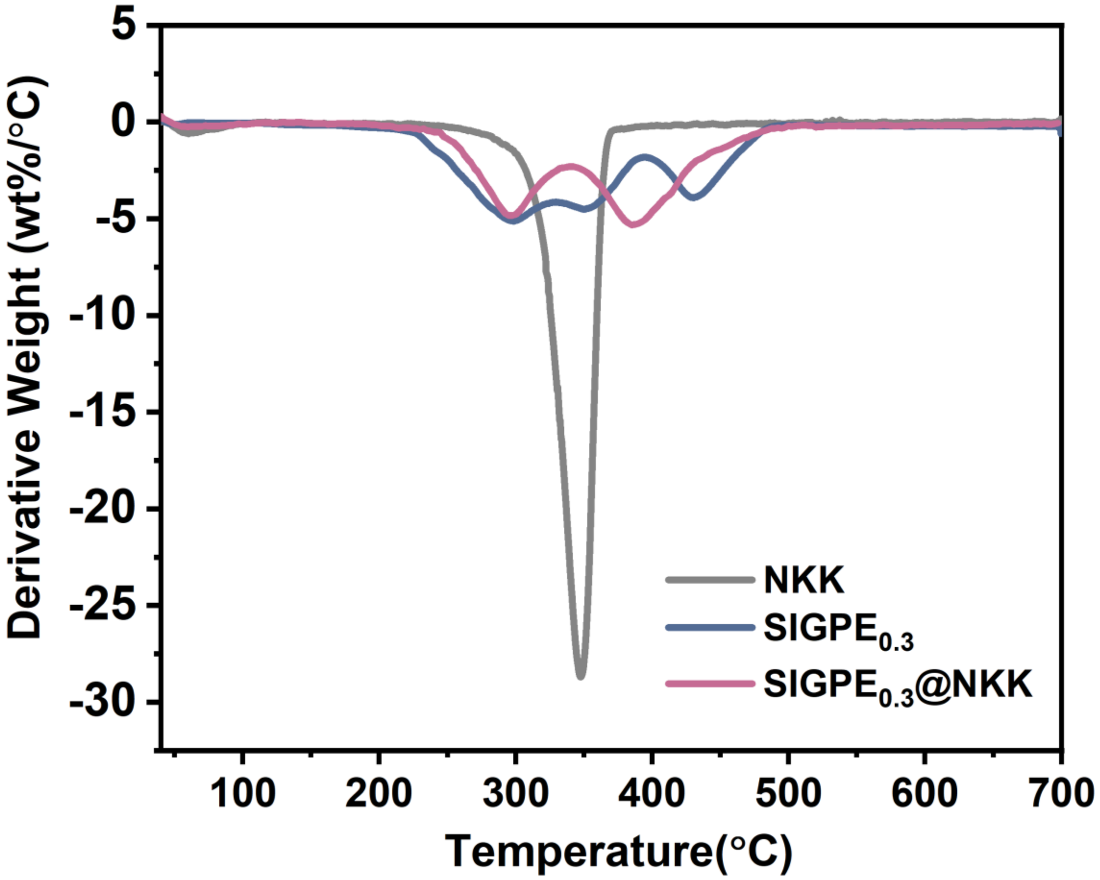

Figure S15. DTG cruves of SIGPE$_{0.3}$@NKK, SIGPE$_{0.3}$, and NKK cellulose membrane.

Table S5. The TGA data of SIGPE$_{0.3}$@NKK, SIGPE$_{0.3}$, and NKK cellulose membrane.

Sample	**$T_{5\%}$(°C)**	**T_{max} (°C)**	**v_{max} (wt.%/min)**	**Wt_R^{700} (wt.%)**
SIGPE$_{0.3}$	**248**	**298.6**	**-5.12**	**13.2**
SIGPE$_{0.3}$@ NKK	**264**	**384.1**	**-5.33**	**24.8**
NKK	**286**	**347.7**	**-28.7**	**6.78**

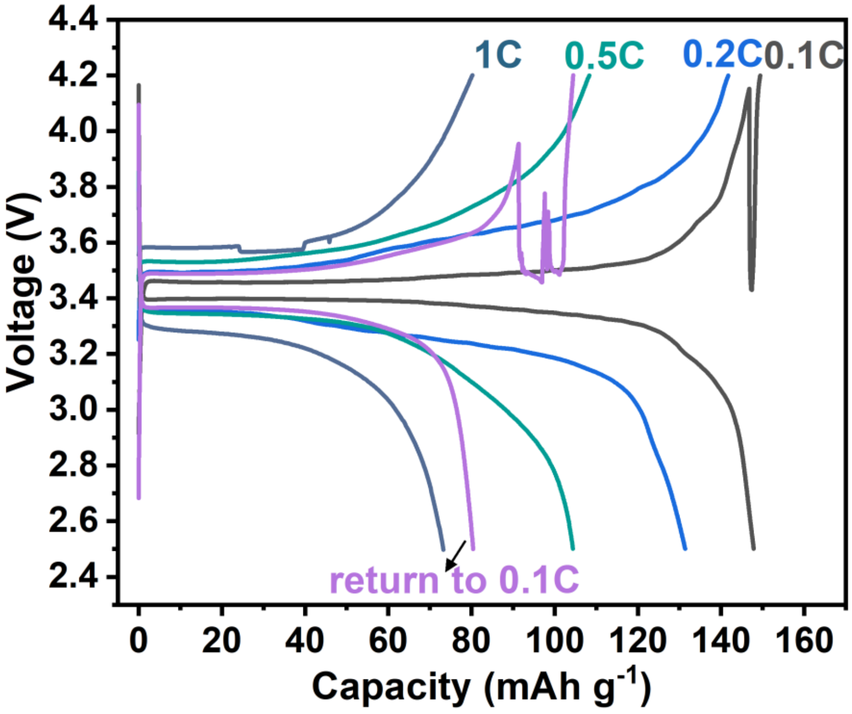

Figure S16. Charge-discharge curves of $LiFePO_4$|LE@NKK |Li pouch cell at 0.2 C.

Table S6. Comparison with the latest state-of-the-art LMBs fabricated by SIGPEs.

SIGPEs[a]	**Years; Journal**	**Polymer matrix**	**σ (S cm^{-1})**	**t_{Li+}**[b]	**Cathode /Anode**	**Cycles; capacity (mAh g^{-1}); capacity retention**
[10]	2023; *ACS Energy Lett.*	Sugar-Derived Polyethers	3.71× 10^{-3}	0.90	NA[c]	NA
[11]	2022; *J. Electrochem. Soc.*	Poly(methoxy-polyethylene glycol acrylate-lithiated 2-acrylamido-2-methylpropane sulfonic acid)	1.7 × 10^{-5}	0.76	LFP/Li (0.2 C)	100; 129; 85%
[12]	2021; *Macromolecules*	Ethylene glycol	2.5 × 10^{-4}	0.93	NA	NA
[13]	2020; *ACS Mater. Lett.*	Poly(tetrahydrofuran)-based	2.5 × 10^{-4}	0.84	LFP/Li (0.1 C)	15; 121; 100%
[14]	2020; *Adv. Mater.*	Lithium tetrakis(4-(chloromethyl)-2.3.5.6tetrafluorophenyl)borate with cis-2-butene-1,4-diol	1.5 × 10^{-4}	0.95	LFP/Li (0.5 C)	100; 102; 84%
[15]	2020; *Solid State Ionics*	PVDF-HFP	3.4 × 10^{-5}	0.97	LFP/Li (0.2 C)	100; 152.8; 97%
[16]	2020; *Polymer*	P(MPEGA-AMPSLi) and PVDF-HFP	2.8× 10^{-5}	0.75	LFP/Li (0.2 C)	100; 145.5; 94%
[17]	2019; *Chemelectrochem*	cross-linked PAMPS-Li	1.34× 10^{-5} (60 °C)	0.77	LFP/Li (0.2 C, 60 °C)	100; 126; 90.4%

[18]	2022; *Chem. Eng. J.*	poly(ethylene glycol) diacrylate and PVDF-HFP	1.03×10^{-3}	0.65	LFP^{d}/Li (0.1 C)	100; 127.7; 79%
[19]	2020; *Chem. Eng. J.*	PEGDA	2.74×10^{-5}	0.622	LFP/Li (0.1 C)	150; 101.2; 80%
[20]	2023; *J. Membrane Sci.*	Poly(vinylidene fluoride-co-hexafluoropropylene)	8.15×10^{-5}	0.87	LFP/Li (0.2 C)	450;116.3;78.4%
[21]	2023；*Small*	Poly(vinylidene fluoride-co-hexafluoropropylene)	5.0×10^{-4}	0.93	LFP/Li (0.2 C)	180;144;87.8%
[22]	2024; *Adv. Mater.*	Lignin-based lithium salt	1.3×10^{-4}		LFP/Li (0.2 C)	700; 85;53.7%
[23]	2024； *J. Mater. Chem. A*	Poly(vinylidene fluoride-co-hexafluoropropylene)	1.4×10^{-5} (20 °C) 1.3×10^{-4} (90 °C)		PW/Na (0.1 C)	40;147; NA
[24]	2022; *Adv. Energy Mater.*	Tetraethylene glycol	3.53×10^{-4}	0.92	LFP/Li (0.5 C)	200;146;89%
[25]	2024, *J. Mater. Chem. A*	Lithium 3-chloropropanesulfonyl (trifluoromethanesulfonyl) imide	1.4×10^{-4}	0.97	LFP/Li (0.2 C)	330;145;90%
This work	2024	Polyethylene glycol (PEG)	1.4×10^{-4}	0.85	LFP/Li (0.2 C)	300; 114.4; 87% (1000; 78.8; 58.9%)

[a] SIGPEs: single-ion conductor gel polymer electrolytes; [b] t_{Li+}: lithium ion transference number; [c] NA: not available; [d] LFP :$LiFePO_4$

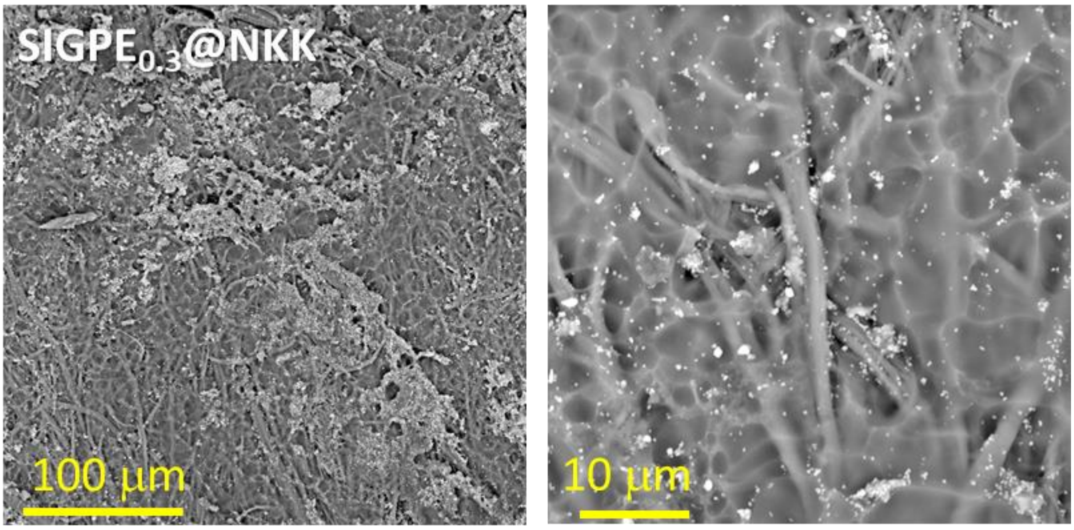

Figure S17. The SEM images of lithium metal anodes after cycling test.

The SEM images of cycled SIGPE$_{0.3}$@NKK show an intact surface morphology, and the SIGPE$_{0.3}$ tightly encapsulates the NKK fibers, indicating that the crosslinked network of SIGPE$_{0.3}$@NKK is stable towards lithium metal after cycling. Those results reflect that the 3D crosslinked network structure leads to a uniform Li deposition and inhibits dendritic Li growth.

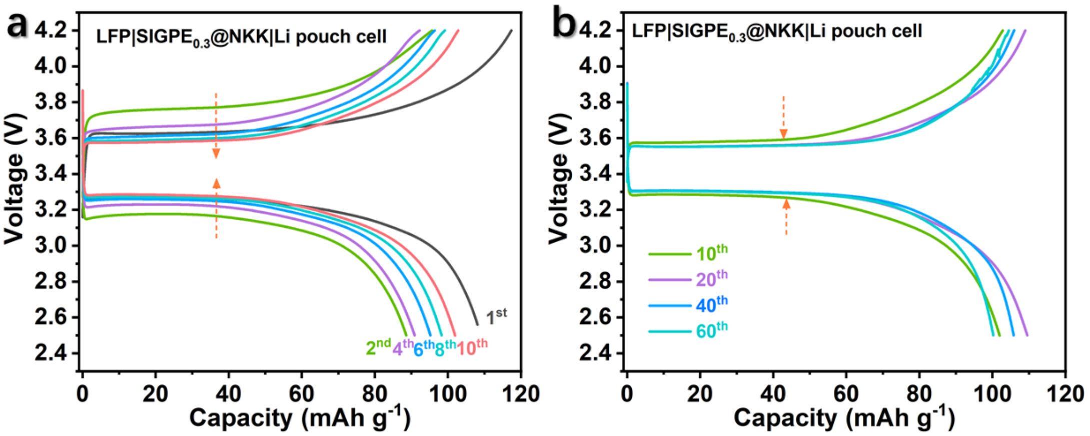

Figure S18. Charge/discharge curves of $LiFePO_4$|$SIGPE_{0.3}$@NKK |Li pouch cell at 0.2 C (a) 1-10 cycles, (b) 10-60 cycles.

In the first 10 cycles, the polarization voltage decreases with the number of cycles, suggesting a reduction of the interfacial impedance; after the 10^{th} cycle, the polarization voltage tends to stabilize. This is because the pouch battery is self-made with insufficient vacuum sealing, resulting in poor interfacial contact and high interfacial contact impedance at the early period. With repeated charging and discharging, the volume of the electrode changes and the effective contact area between the electrolyte and the electrode gradually increases, leading to a decrease in the interfacial contact impedance and an increase in capacity.

References

[1] H.J.C. Berendsen, D.v.d. Spoel, R.v. Drunen, GROMACS: A message-passing parallel molecular dynamics implementation, Computer Physics Communications 91 (1995) 43-56. https://doi.org/https://doi.org/10.1016/0010-4655(95)00042-E.

[2] D. Van Der Spoel, E. Lindahl, B. Hess, G. Groenhof, A.E. Mark, H.J.C. Berendsen, GROMACS: Fast, flexible, and free, Journal of Computational Chemistry 26(16) (2005) 1701-1718. https://doi.org/10.1002/jcc.20291.

[3] S. Pall, M.J. Abraham, C. Kutzner, B. Hess, E. Lindahl, Solving Software Challenges for Exascale, 2015. https://doi.org/10.1007/978-3-319-15976-8.

[4] M.J. Abraham, T. Murtola, R. Schulz, S. Páll, J.C. Smith, B. Hess, E. Lindahl, GROMACS: High performance molecular simulations through multi-level parallelism from laptops to supercomputers, SoftwareX 1-2 (2015) 19-25. https://doi.org/10.1016/j.softx.2015.06.001.

[5] L. Martínez, R. Andrade, E.G. Birgin, J.M. Martínez, PACKMOL: A package for building initial configurations for molecular dynamics simulations, Journal of Computational Chemistry 30(13) (2009) 2157-2164. https://doi.org/10.1002/jcc.21224.

[6] W.L. Jorgensen, D.S. Maxwell, J. Tirado-Rives, Development and Testing of the OPLS All-Atom Force Field on Conformational Energetics and Properties of Organic Liquids, Journal of the American Chemical Society 118 (1996) 11225-11236. https://doi.org/https://doi.org/10.1021/ja9621760.

[7] T. Lu, F. Chen, Multiwfn: A multifunctional wavefunction analyzer, Journal of Computational Chemistry 33(5) (2011) 580-592. https://doi.org/10.1002/jcc.22885.

[8] S. Grimme, J. Antony, S. Ehrlich, H. Krieg, A consistent and accurateab initioparametrization of density functional dispersion correction (DFT-D) for the 94 elements H-Pu, The Journal of Chemical Physics 132(15) (2010). https://doi.org/10.1063/1.3382344.

[9] F. Neese, Software update: The ORCA program system-Version 5.0, WIREs Computational Molecular Science 12(5) (2022). https://doi.org/10.1002/wcms.1606.

[10] E.L. Daniels, J.R. Runge, M. Oshinowo, H.S. Leese, A. Buchard, Cross-Linking of Sugar-Derived Polyethers and Boronic Acids for Renewable, Self-Healing, and Single-Ion Conducting Organogel Polymer Electrolytes, ACS Applied Energy Materials 6(5) (2023) 2924-2935. https://doi.org/10.1021/acsaem.2c03937.

[11] X. Shen, T. Hu, Y. Zeng, X. Huang, P. Zhang, J. Zhao, Core-Shell Structured Gel Polymer Electrolyte with Single-Ion Conducting and Thermal Stability Bifunction for Lithium-Ion Batteries, Journal of The Electrochemical Society 169(7) (2022) 070505. https://doi.org/10.1149/1945-7111/ac79d5.

[12] M.L. Aubrey, J.C. Axelson, K.E. Engler, J.R. Long, Dependence of Linker Length and Composition on Ionic Conductivity and Lithium Deposition in Single-Ion Conducting Network Polymers, Macromolecules 54(16) (2021) 7582-7589. https://doi.org/10.1021/acs.macromol.1c00911.

[13] H.O. Ford, B. Park, J. Jiang, M.E. Seidler, J.L. Schaefer, Enhanced Li^+ Conduction within Single-Ion Conducting Polymer Gel Electrolytes via Reduced Cation-Polymer Interaction, ACS Materials Letters 2(3) (2020) 272-279. https://doi.org/10.1021/acsmaterialslett.9b00510.

[14] D.M. Shin, J.E. Bachman, M.K. Taylor, J. Kamcev, J.G. Park, M.E. Ziebel, E. Velasquez, N.N. Jarenwattananon, G.K. Sethi, Y. Cui, J.R. Long, A Single‐Ion Conducting Borate Network Polymer as a Viable Quasi‐Solid Electrolyte for Lithium Metal Batteries, Advanced Materials 32(10) (2020) 1905771. https://doi.org/10.1002/adma.201905771.

[15] H. Li, X. Shen, H. Hua, J. Gao, Z. Wen, X. Wang, L. Peng, D. Wu, P. Zhang, J. Zhao, A novel single-ion conductor gel polymer electrolyte prepared by co-irradiation grafting and electrospinning process, Solid State Ionics 347 (2020) 115246. https://doi.org/10.1016/j.ssi.2020.115246.

[16] X. Shen, H. Hua, H. Li, R. Li, T. Hu, D. Wu, P. Zhang, J. Zhao, Synthesis and molecular dynamic simulation of a novel single ion conducting gel polymer electrolyte for lithium-ion batteries, Polymer 201 (2020) 122568. https://doi.org/10.1016/j.polymer.2020.122568.

[17] X. Shen, L. Peng, R. Li, H. Li, X. Wang, B. Huang, D. Wu, P. Zhang, J. Zhao, Semi-Interpenetrating Network-Structured Single-Ion Conduction Polymer Electrolyte for Lithium-Ion Batteries, Chemelectrochem 6(17) (2019) 4483-4490. https://doi.org/10.1002/celc.201901045.

[18] X. Zeng, L. Dong, J. Fu, L. Chen, J. Zhou, P. Zong, G. Liu, L. Shi, Enhanced interfacial stability with a novel boron-centered crosslinked hybrid polymer gel electrolytes for lithium metal batteries, Chemical Engineering Journal 428 (2022) 131100, https://doi.org/10.1016/j.cej.2021.131100.

[19] X. Guan, Q. Wu, X. Zhang, X. Guo, C. Li, J. Xu, In-situ crosslinked single ion gel

polymer electrolyte with superior performances for lithium metal batteries, Chemical Engineering Journal 382 (2020) 122935, https://doi.org/10.1016/j.cej.2019.122935.

[20] X. Jing, Z. Hu, J. Qin, X. Jiang, M. Wang, S. Huo, S. Zhang, J. Wang, Y. Zhang, Highly conductive and mechanically robust single-ion conducting polymer electrolyte membranes with a high concentration of charge carriers for dendrite-proof lithium metal batteries, Journal of Membrane Science 688 (2023). https://doi.org/10.1016/j.memsci.2023.122118.

[21] Z. Li, L. Wang, Y. Liu, M. Yu, B. Liu, Y. Men, Z. Sun, W. Hu, G. Zhu, Single-Ion Polymer Electrolyte Based on Lithium‐Rich Imidazole Anionic Porous Aromatic Framework for High Performance Lithium‐Ion Batteries, Small 19(41) (2023). https://doi.org/10.1002/smll.202302818.

[22] Y. Liu, P. Wang, Z. Yang, L. Wang, Z. Li, C. Liu, B. Liu, Z. Sun, H. Pei, Z. Lv, W. Hu, Y. Lu, G. Zhu, Lignin Derived Ultrathin All-Solid Polymer Electrolytes with 3D Single-Ion Nanofiber Ionic Bridge Framework for High Performance Lithium Batteries, Advanced Materials 36(27) (2024). https://doi.org/10.1002/adma.202400970.

[23] C. Wunder, T.-L. Lai, E. Šić, T. Gutmann, E. De Vito, G. Buntkowsky, M. Zarrabeitia, S. Passerini, Sodium 4-styrenesulfonyl(trifluoromethanesulfonyl)imide-based single-ion conducting polymer electrolyte incorporating molecular transporters for quasi-solid-state sodium batteries, Journal of Materials Chemistry A 12(32) (2024) 20935-20946. https://doi.org/10.1039/d4ta02329c.

[24] H. Li, Y. Du, Q. Zhang, Y. Zhao, F. Lian, A Single-Ion Conducting Network as Rationally Coordinating Polymer Electrolyte for Solid‐State Li Metal Batteries,

Advanced Energy Materials 12(13) (2022). https://doi.org/10.1002/aenm.202103530.

[25] Z. Li, Y. Liu, X. Liang, M. Yu, B. Liu, Z. Sun, W. Hu, G. Zhu, A single-ion gel polymer electrolyte based on polyimide grafted with lithium 3-chloropropanesulfonyl (trifluoromethanesulfonyl) imide for high performance lithium ion batteries, Journal of Materials Chemistry A 11(4) (2023) 1766-1773. https://doi.org/10.1039/d2ta09097j.